Received: 22 January 2024 | Revised: 13 November 2024 | Accepted: 19 December 2024

DOI: 10.1002/mco2.70104

ORIGINAL ARTICLE

MedComm Open Access WILEY

Early-life antibiotic exposure aggravates hepatic steatosis through enhanced endotoxemia and lipotoxic effects driven by gut *Parabacteroides*

Xi Zhang[1,2,3,4] | **Darren Chak Lun Chan**[4] | **Jie Zhu**[1] | **Daniel Zhen Ye Sin**[2,3] | **Ye Peng**[1,2,3] | **Matthew Kwok Leong Wong**[1] | **Wenyi Zhu**[1,3,7] | **Yee Tsui**[4] | **Andrea M. Haqq**[5] | **Joseph Y. Ting**[5] | **Anita Kozyrskyj**[5] | **Francis Ka Leung Chan**[1,6] | **Siew Chien Ng**[1,3,7,#] | **Hein Min Tun**[1,2,3,*,#]

[1]Microbiota I-Center (MagIC), Hong Kong SAR, China

[2]Jockey Club School of Public Health and Primary Care, Faculty of Medicine, The Chinese University of Hong Kong, Hong Kong SAR, China

[3]Li Ka Shing Institute of Health Sciences, Faculty of Medicine, The Chinese University of Hong Kong, Hong Kong SAR, China

[4]HKU-Pasteur Research Pole, School of Public Health, LKS Faculty of Medicine, The University of Hong Kong, Hong Kong SAR, China

[5]Department of Pediatrics, University of Alberta, Edmonton, Canada

[6]Centre for Gut Microbiota Research, The Chinese University of Hong Kong, Hong Kong SAR, China

[7]Department of Medicine and Therapeutics, Faculty of Medicine, The Chinese University of Hong Kong, Hong Kong SAR, China

***Correspondence**
Hein Min Tun, Microbiota I-Center (MagIC), Hong Kong SAR, China.
Email: heintun@cuhk.edu.hk

Funding information
Research Grants Council of the Hong Kong Special Administrative Region, China, Grant/Award Numbers: 27117022, 14113923; InnoHK, The Government of Hong Kong, Special Administrative Region of the People's Republic of China; The start-up research grant of The Chinese University of Hong Kong

Abstract

Compelling evidence supports a link between early-life gut microbiota and the metabolic outcomes in later life. Using an early-life antibiotic exposure model in BALB/c mice, we investigated the life-course impact of prenatal and/or postnatal antibiotic exposures on the gut microbiome of offspring and the development of metabolic dysfunction-associated steatotic liver disease (MASLD). Compared to prenatal antibiotic exposure alone, postnatal antibiotic exposure more profoundly affected gut microbiota development and succession, which led to aggravated endotoxemia and metabolic dysfunctions. This was primarily resulted from the overblooming of gut *Parabacteroides* and hepatic accumulation of cytotoxic lysophosphatidyl cholines (LPCs), which acted in conjunction with LPS derived from *Parabacteroides distasonis* (LPS_PA) to induce cholesterol metabolic dysregulations, endoplasmic reticulum (ER) stress and apoptosis. Integrated serum metabolomics, hepatic lipidomics and transcriptomics revealed enhanced glycerophospholipid hydrolysis and LPC production in association with the upregulation of PLA2G10, the gene controlling the

[#]Siew Chien Ng and Hein Min Tun are Senior Authors.

expression of the group X secretory Phospholipase A2s (sPLA2-X). Taken together, our results show microbial modulations on the systemic MASLD pathogenesis and hepatocellular lipotoxicity pathways following early-life antibiotic exposure, hence help inform refined clinical practices to avoid any prolonged maternal antibiotic administration in early life and potential gut microbiota-targeted intervention strategies.

KEYWORDS
antibiotics, early life, gut microbiota, lipotoxicity, metabolic dysfunction-associated steatotic liver disease

1 | INTRODUCTION

The early-life gut microbiome plays an important role in the healthy development of the immune system and metabolism of the host. Indeed, early-life gut dysbiosis affects the risks of developing multiple chronic diseases in later life including obesity and liver steatosis.[1,2] Several prenatal and postnatal factors affect gut microbiota succession and development in neonates such as delivery mode, neonatal diets (e.g., breastfeeding and solid food intake), and antibiotic exposure,[3–5] the latter of which is an increasing concern. An estimated 20–30% of pregnant women and their newborns worldwide receive antibiotics to prevent severe neonatal bacterial infections and/or postpartum infections following cesarean delivery; most infants receive antibiotics in their first year of life.[6,7] Worryingly, gut microbiota dysbiosis in early life may lead to the impaired development of mucosal and systemic immunities and increase the risks of suffering from immune-mediated diseases and metabolic outcomes in later life, including metabolic dysfunction-associated steatotic liver disease (MASLD).[6,8–11]

MASLD, formerly known as nonalcoholic fatty liver disease, is a metabolic disorder where hepatic steatosis is accompanied by overweight/obesity, type 2 diabetes mellitus, or other metabolic disorders.[12] The global prevalence of MASLD is currently estimated to be 39.22%,[13] and around 20% of patients rapidly and asymptomatically progress to advanced fibrosis,[14] a leading cause for hepatocellular carcinoma and cardiovascular complications.[15] Sufferers with chronic liver disease are closely associated with the development of severe COVID-19.[16] Of concern, there is no specific pharmacological therapy currently available. The etiology of MASLD consists of complex interactions between environmental factors, genetics, and metabolic risk factors including obesity and microbiome dysbiosis.[17–19] Microbiome dysbiosis has been linked to dysregulated lipid metabolism[20–24]; abnormal lipid and cholesterol metabolism then drives steatosis progression through lipotoxic effects [e.g., the induction of endoplasmic reticulum (ER) stress] that cause hepatocellular damage and ultimately cell death.[25,26] Direct antibiotic exposure in early life has been shown to enhance hepatic metabolic disorders, adiposity, and immunity defects through gut microbiome dysbiosis.[27–29] However, the respective contributions of prenatal and/or postnatal antibiotic exposure on the development of metabolic syndrome in offspring have not yet been clarified. While several human studies linked early-life antibiotic exposure to childhood obesity risk and infant microbiota alterations,[30–32] the life-long effect of maternal antibiotic exposure remains unknown, probably due to the long timespan and vague information of the duration and the type of antibiotic usage.

Given the lack of suitable clinical evidence, we therefore implemented a BALB/c mouse model to comparatively characterized both short- and long-term impacts of prenatal and postnatal maternal antibiotic exposure on the gut microbiome of offspring. Penicillin V was administered to female mice, as this β-lactam antibiotic is one of the most frequently prescribed antibiotics worldwide to prevent severe bacterial infections during pregnancy or following cesarean delivery.[33,34] The hepatocellular pathogenic responses were investigated through a multiomics analysis and associated with the cytotoxic lipids lysophosphatidyl cholines (LPCs) and microbiota perturbations generated by early-life antibiotic exposure. We then evaluated the enrichment of *Parabacteroides* on gut barrier function, the induction of endotoxemia, and the subsequent metabolic dysfunctions and hepatic cell death effect.

2 | RESULTS

2.1 | Early-life antibiotic exposure disrupted the intergenerational succession of gut microbiota from dams to offspring

We longitudinally monitored the gut microbiota profiles of mice exposed to antibiotics through maternal antibiotic

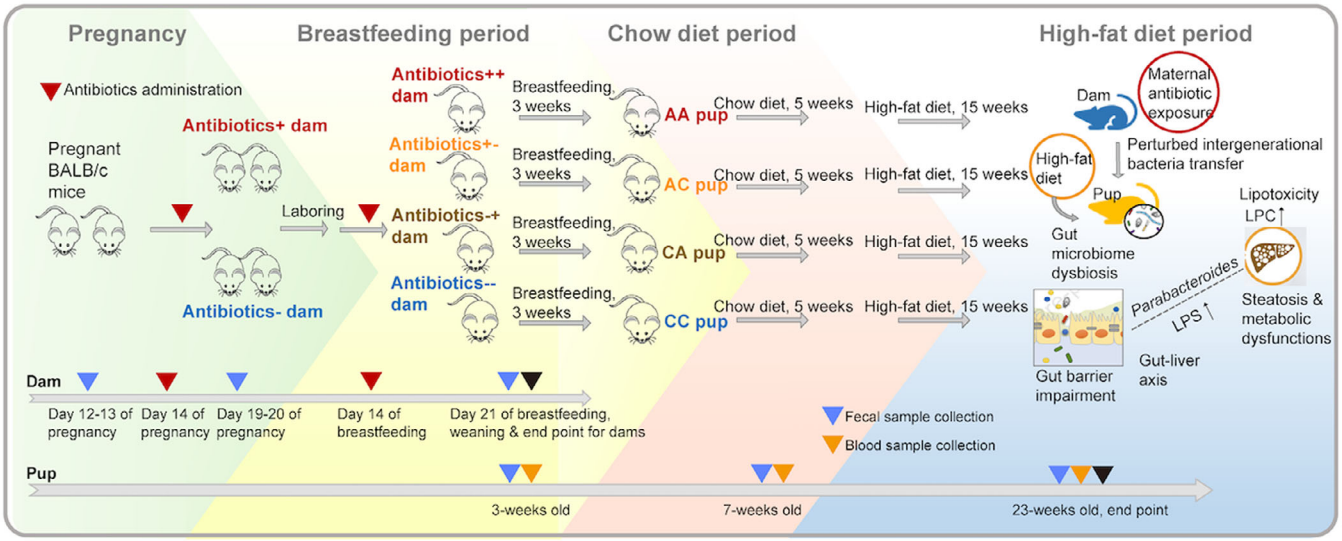

FIGURE 1 Schematic overview of study design. Assigned female BALB/c mice were exposed to Penicillin V via drinking water at 0.25 mg/mL in their late pregnancy (the last week prior to laboring), late lactation period (the last week prior to weaning), or during both the pregnancy and breastfeeding period. Pups were weaned at Day 21 and retained males were then assigned into 4 groups according to their early-life antibiotic exposure status. All groups of pups underwent a 10% kcal fat standard chow diet period for 5 weeks, then shifted to a 45% kcal fat high-fat diet until the end of the experiment. Fecal samples were collected from each dam before and after antibiotic administration during pregnancy and the lactation period, and from each pup during the breastfeeding, chow diet, and high-fat diet periods for gut microbiota profiling analysis. All the mice were sacrificed at the endpoint for tissue collection. LPS, lipopolysaccharides; LPC, lysophosphatidyl choline.

administration prenatally and/or postnatally (Figure 1). To determine whether maternal antibiotic administration affected the intergenerational transfer of gut microbiota from dam to pup, we analyzed the shared bacterial taxa between the baseline pregnancy microbiota of dams and their respective offspring's microbiota during the breastfeeding period. Consistent with previous studies,[35] the similarities of gut microbiota profiles varied among dam-pup dyads in different antibiotic exposure groups (Figure 2, Table S1). The gut microbiota of the control group of pups born by dams without maternal antibiotic exposure (CC) demonstrated the highest transfer fidelity, as represented by a larger number of shared taxa and the occurrence of intergenerational transfer events among all dam-pup dyads (Figure 2A, Table S1). While the transfer fidelity of the gut microbiota in the AC (pups born by dams with only prenatal antibiotic exposure) groups were at a comparable level to that of the CC group, those of the CA (pups born by dams with only postnatal antibiotic exposure) and AA (pups born by dams with both prenatal and postnatal antibiotic exposure) groups were largely dampened, as indicated by a smaller number of shared taxa between generations (Figure 2B, Table S1) and significantly higher dissimilarities in the overall gut microbiota composition (Figure 2C). For the dam-pup pairs of the CC and AC groups, the majority of the bacterial taxa were almost identical. However, almost half of the taxa originally present in dams, including *Lactobacillus*, *Muribaculum*, *Alistipes*, and *Odoribacter*, were either diminished or depleted in their respective offspring in the CA and AA groups (Figure 2A). The gut microbiota of the AA group, which was exposed to antibiotics for the longest duration (during both prenatal and postnatal periods), showed the least transfer fidelity.

2.2 | Short- and long-term perturbations in gut microbiota of offspring followed early-life maternal antibiotic administration

We found both short- and long-term effects of early-life maternal antibiotic administration on the gut microbiota of offspring with different diets at both the neonatal and postweaning periods (Figure 3A-D). Compared to the CC group, early-life antibiotic exposure resulted in the depletion of microbiota species richness (Figure 3A). Moreover, the magnitude of microbiota depletion in the CA and AA groups was greater compared to that of AC group (Figure 3A). Both principal coordinates analysis (PCoA) and canonical correlation analysis (CCA) indicated that the gut microbiota composition of the AA group was similar to that of the CA group, while the gut microbiota composition of the AC group was more similar to that of the

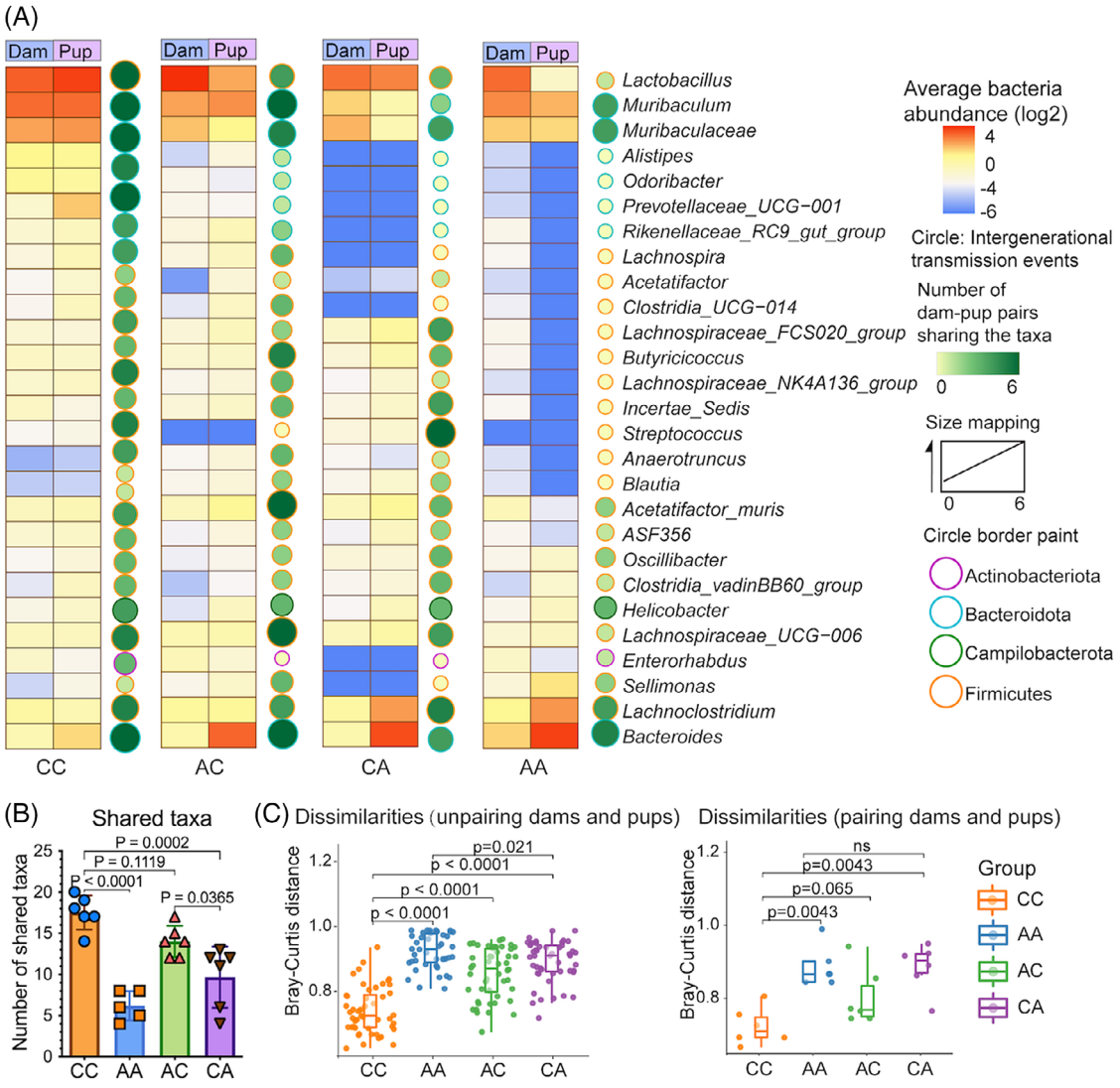

FIGURE 2 Intergenerational microbiota transfer fidelities varied in mice with prenatal and/or postnatal antibiotic exposure. (A) Intergenerational distribution and expression of each bacteria taxa. Each pup and dam were paired up to identify the number of shared bacterial taxa and their abundances. The heatmap squares were generated based on the average abundance of taxa from 16S rRNA microbiome profiling. The size of the circle is proportional to the number of dam-pup pairs with intergenerational transfer of the respective taxa. (B) The number of shared taxa among paired dams and pups. (C) Bray–Curtis distance calculated by grouping all dams and pups under each treatment together (left panel) and pairing each dam and pup for matched comparison (right panel). Data point collected during breastfeeding (when pups reached 3 weeks) were used for analysis. The number of dam-pup dyads for CC, AA, AC, CA group was 6, 5, 6, 6, respectively. *p* value was calculated by a Wilcoxon's rank-sum test. AA, pups born by dams with prenatal and postnatal antibiotic exposure; AC, pups born by dams with only prenatal antibiotic exposure; CA, pups born by dams with only postnatal antibiotic exposure; CC, pups born by dams without antibiotic exposure.

CC group (Figure 3C). *Firmicutes* and *Bacteroidetes* were the predominant bacterial phyla in all groups. To identify differential genera associated with postnatal antibiotic exposure, we used linear discriminant analysis effect size (LEfSE) to compare bacterial abundances at the genus level. The abundances of multiple bacterial genera such as *Rikenellaceae_RC9_gut_group*, *Alistipes*, and *Lactobacillus* were consistently diminished in the CA and AA groups under both breastfeeding and HFD. The abundances of *Enterorhabdus*, *Bacteroides*, *Parabacteroides*, *Lachnoclostridium*, *Lachnospiraceae_FCS020_group*, *Staphylococcus*, *Lachnospiraceae_UCG-004*, *Muribaculaceae*, and *Enterococcus* were consistently enriched in the AA or CA groups [linear discriminant analysis (LDA) score > 2, $p < 0.05$] (Figure 3D).

By contrast, in dams, the effect of antibiotic administration was reversible: the altered gut microbiota returned to the baseline profile after the removal of antibiotic administration in different mouse groups (Figure S1).

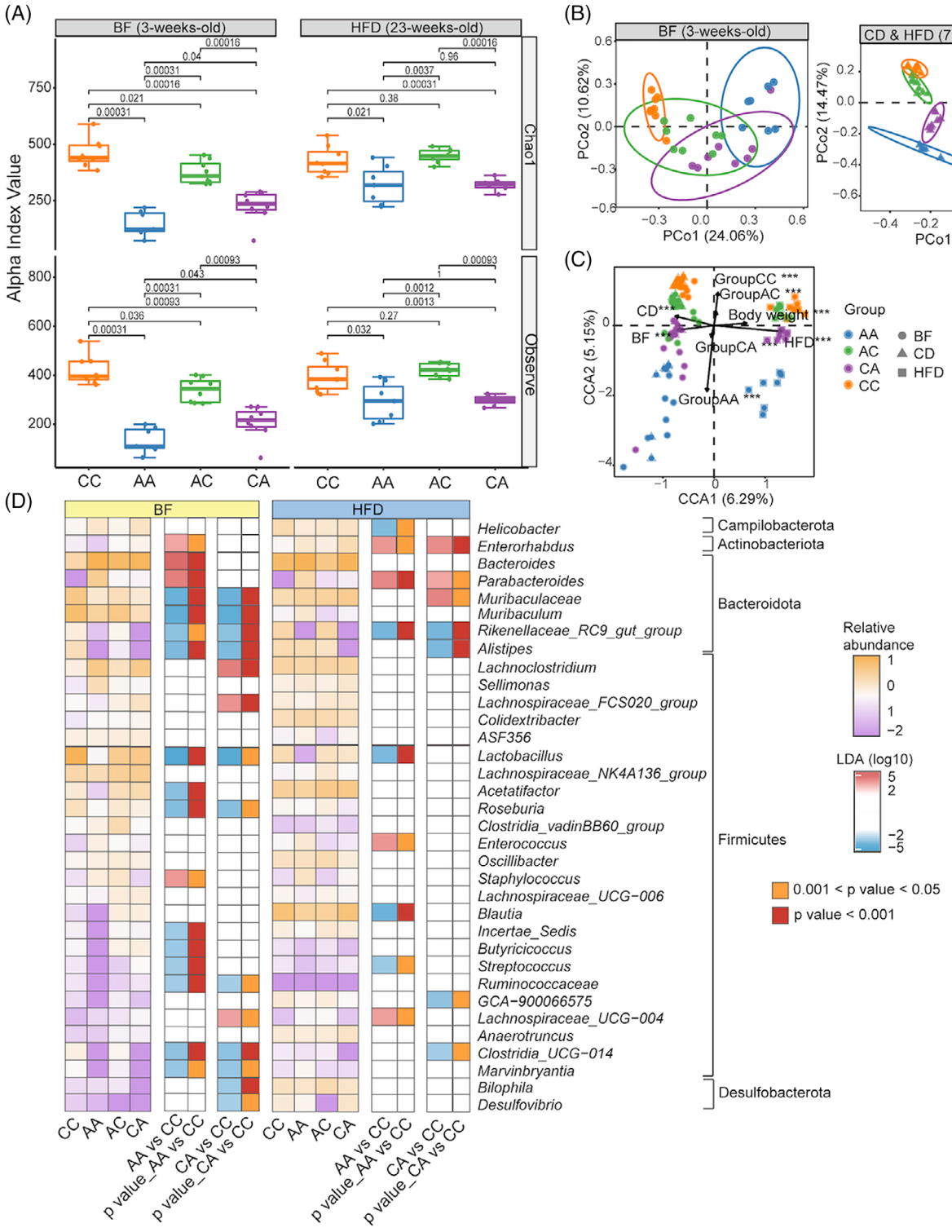

FIGURE 3 Prenatal and/or postnatal antibiotic exposure altered the gut microbiome composition and diversity in offspring mice. (A) α-diversity of the gut flora of pups was calculated by Chao1 and Observe. (B, C) Principal coordinates analysis (PCoA) (B) and Canonical correlation analysis (C) showing the similarities in the gut microbiome community structures among pups. (D) Linear discriminant analysis effect size (LEfSe) showing the bacterial taxa altered by early-life antibiotic exposure under dietary effects. The relative abundance of each taxon was graphed in the heatmap. We considered taxa with linear discriminant analysis (LDA) > 2 and $p < 0.05$ to be significant. The most significantly representative taxa were marked with blue (more abundant in CC) or red (more abundant in AA or CA). The number of pups within CC, AA, AC, CA group was 6, 5, 6, 6, respectively. BF samples were collected when pups were 3 weeks old; CD samples were collected when pups were 7 weeks old; HFD samples were collected when pups were 23 weeks old. BF, breastfeeding period; CD, chow diet period; HFD, high-fat diet period.

2.3 | Early-life antibiotic exposure aggravated metabolic dysfunction through microbiome-mediated mechanisms

While HFD treatment did not significantly change body weight (Figure S2), we observed a trend of elevated serum lipopolysaccharides (LPS) in mice with early-life antibiotic exposure, albeit not statistically significant (Figure 4A). Regardless, HFD treatment reduced levels of tight junction protein occludin in the ileum (Figure 4B and C), raised levels of serum cholesterol, triglyceride, low-density lipoprotein cholesterol (LDL-C), cholesterol/high-density lipoprotein cholesterols (HDL-C) ratio (Figure 4D) and hepatic lipid deposition (Figure 4E and F) in mice exposed to antibiotics in early life. Ileal barrier impairment, metabolic endotoxemia, and hepatic steatosis were more prominent in mice with postnatal antibiotic exposure (AA and CA mice) compared to mice with prenatal antibiotic exposure alone. Liver transcriptomics analysis indicated imbalanced lipid synthesis and utilization in antibiotics-exposed mice, which may have contributed to steatosis development. Genes regulating cholesterol synthesis [3-Hydroxy-3-Methylglutaryl-CoA Reductase (HMGCR), 3-Hydroxy-3-Methylglutaryl-CoA Synthase 1 (HMGCS1), Lanosterol Synthase (LSS)] tended to increase in the livers of AA mice under HFD (Figure 4G). While the gene regulating cholesterol export and utilization, including ATP Binding Cassette Subfamily G Member 1 (ABCG1), and several rate-limiting enzymes in cholesterol metabolism including Cholesterol 7α-hydroxylase (CYP7A1), Cytochrome P450 Family 7 Subfamily B Member 1 (CYP7B1) and Cytochrome P450 Family 7 Subfamily A Member 1 (CYP27A1), were transcriptionally downregulated in AA group compared to mice without early-life antibiotic exposure (CC) (Figure 4G). Interestingly, hepatic expression of CYP7A1 decreased in HFD-fed mice exposed to antibiotics in early life ($p = 0.022$) (Figure 4G), which indicated the modulation of microbiome perturbations on inherent metabolic capacity which drives the phenotypic HFD resistance.[36–38]

2.4 | Multiomic analysis revealed the disturbance of glycerophospholipid metabolism and the lipotoxic effects of hepatic lysophosphatidyl choline (LPC) in triggering ER stress and apoptosis

To better understand the way in which the microbiome contributed to hepatic pathogenesis, we integrated serum metabolomics, hepatic lipidomics and transcriptomics to identify microbial markers associated with the dysregulated glycerophospholipid metabolism and the consequent lipotoxic effects and hepatocellular damage. A total of 71 differentially expressed lipids were identified among the different mice groups, with the majority of the lipids being glycerophospholipids (Figure 5A). Certain lipotoxic lipid groups (ER stress and apoptosis inducers), including diglycerides (DG) and LPCs,[25,26,39] were significantly elevated in mice with early-life antibiotic exposure (Figure S3A). Lysophospholipids, including LPCs, are known to be produced along with fatty acids by the Phospholipase A_2 (PLA_2) through hydrolyzing glycerophospholipids (Figure 5B). Interestingly, we observed a significant increase of gastric PLA2G10—a gene encoding group X secretory PLA_2 ($sPLA_2$-X) (Figure 5C), which might have contributed to the dysregulated glycerophospholipid metabolism and LPC production.[40] As previous studies suggested that LPS induces gastric permeability in parallel with the luminal secretion of PLA_2 and LPCs,[40] we examined the correlations between LPS-expressing gut microbial taxa and the elevated lipid species (Figure S3B). *Parabacteroides*, an LPS-producing Gram-negative bacterium consistently enriched in both breastfed and HFD-fed mice with postnatal antibiotic exposure, was positively correlated with LPC and DG levels (Figure S3B).

LPCs that were positively correlated with *Parabacteroides* were further investigated by integrating them into a lipid-gene network (Table S2). Consistent with our hypothesis, the majority of the genes related to ER stress, apoptosis, and the phosphatidylinositol-3-kinase (PI3K)-AKT pathway were positively correlated with the selected LPCs (Figure S3C). Consistent with prior studies,[41,42] the dominant function of these LPCs tended to be lipoapoptotic rather than pro-inflammatory, as evidenced by their activation of executor caspases and transcriptional suppression of proinflammatory markers [e.g., C–C motif ligand 2 (CCL2), C-X-C motif chemokine ligand 1, 2, and 10 (CXCL1, CXCL2, and CXCL10), interleukin (IL)-1β and IL-18] (Figure 5E). Moreover, compared to antibiotic-naive mice (CC), the serum level of the pro-inflammatory cytokine tumor necrosis factor (TNF)-α was significantly lower in HFD-fed mice with early-life antibiotic exposure ($p < 0.05$) (Figure S4). Associated with the presence of *Parabacteroides*, hepatocellular responses in HFD-fed mice with both prenatal and postnatal antibiotic exposure (AA) were more largely perturbed (AA: 12 LPCs, 4 fatty acids and 153 correlations; CA: 3 LPCs, 1 fatty acid and 85 correlations; AC: 7 LPCs, 3 fatty acids and 109 LPC-gene correlations) (Figure 5E).

As LPCs with different structures could function diversely in cholesterol biosynthesis and determining MASLD phenotype,[43] we matched the LPCs with their cognate fatty acids (Figure 5D) to further pinpoint those originated from the dysregulated glycerophospholipid metabolism mediated by $sPLA_2$-X. Among all the matched

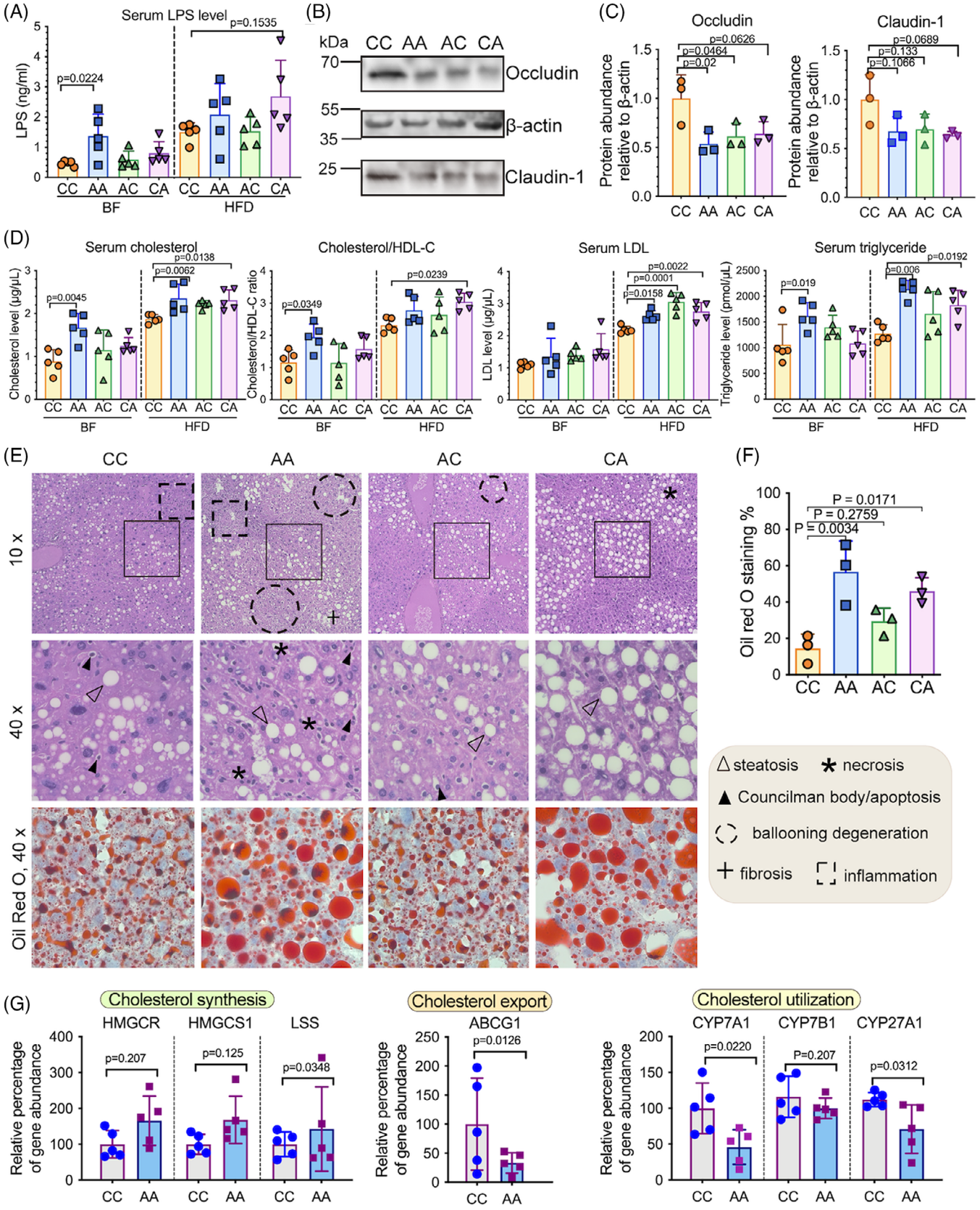

FIGURE 4 Postnatal antibiotic exposure aggravated the metabolic dysfunction in HFD-fed mice. (A) Serum LPS level of pups before (during breastfeeding (BF)) and after HFD treatment. Data represented as mean ± SEM, $n = 5$, one-way ANOVA. (B, C) Western blot image (B) and protein density quantification (C) of BALB/c pups' ileal tight junction protein expression after HFD treatment. The abundance of occludin and claudin-1 in each sample (C) was quantified relative to β-actin in western blot images by ImageJ. Data represented as

pairs of fatty acids and LPCs, only behenic acid (22:0) and LPC (22:0) were simultaneously elevated in mice with antibiotic exposure and potentially generated through the action of $sPLA_2$-X (Figure 5E). The interactive networks included the activation of ER chaperons [heat shock protein (HSP) 40, HSP90B1], and apoptotic markers (p38, caspases).

2.5 | *Parabacteroides* augmented LPS release and the pathogenesis of MASLD through metabolic perturbations and lipotoxicity effect in in vitro models

To investigate how overblooming of *Parabacteroides* following early-life antibiotic exposure exacerbated the pathogenesis of MASLD, we first tested the functional components of *Parabacteroides* that affect gut barrier function and LPS release. To that end, filtered *Parabacteroides distasonis* (PA) supernatant, heat-inactivated PA, and LPS extract of PA (LPS_PA) were added into the differentiated human intestinal epithelial cells HRT18 in Transwells to compare their effect on abundance and integrity of tight junction proteins (Figure 6A). Compared to heat-inactivated PA, PA supernatant more dramatically decreased the expression of Claudin-1 (not significantly) and Occludin ($p = 0.0041$) (Figure 6B, upper panels). LPS_PA significantly decreased the expression of Claudin-1 ($p = 0.0263$) (Figure 6B, lower panels). Of note, LPS_PA induced the largest increase of monolayer permeability (over 58.5%, $p < 0.0001$) amongst all PA components as measured by transepithelial electric resistance (TEER) (Figure 6C and D), and allowed more efficient LPS translocation thereafter (Figure 6E). These results strongly hinted that LPS of PA and those released form dampened gut barrier and further facilitated the LPS translocation. Intriguingly, these effects exerted by LPS extract of PA seemed to be comparable with those extracted from *E. coli* (Figure 6B-E).

The consequential effects of LPS_PA on glycerophospholipid metabolism and LPC production were examined (Figure 6F). Conform to our hypothesis, LPS_PA treatment increased the transcriptomic expression of $sPLA_2$-X (PLA2G10) in HRT18 cells (Figure 6G), suggesting an enhanced glycerophospholipid hydrolysis and LPC production.[40] Therefore, we proceeded to investigate the subsequent metabolic perturbations and hepatocelluar damages caused by the overproduction of LPS and LPCs. Our results showed that individually and combinatorially administered LPS_PA and LPC (22:0) overall promoted cholesterol accumulation in Huh7 cells, while there exists a discrepancy of their target genes (Figure 6H). Individually and combinatorially administered LPS_PA and LPC (22:0) both upregulated HMGCR and downregulated ABCG1 to augment cholesterol synthesis and limit cholesterol export (Figure 6H). Interestingly, HMGCS1, LSS and CYP7B1 were only regulated by LPS_PA, while CYP27A1 only responded to LPC (22:0) treatment (Figure 6H). While LPS extracted from *E. coli* could also perturb cholesterol metabolism, it might function through PLA2G10-inpdependent pathways (Figure S6).

The "double-hit" hypothesis proposed massive hepatocellular damage as a "second hit" of MASLD pathogenesis, following the primary lipid accumulation.[44] Our results showed that LPS_PA and LPC (22:0) treatment induced apoptosis in Huh7 cells at similar levels (Figure 6I and J), specifically by triggering ATF6 cleavage and elevating Hsp90b1, followed by the phosphorylation of p38 and the cleavage of the executor caspase (Figure 6J). Collectively, we demonstrated that overblooming of *Parabacteroides* could potentially dampen gut barrier functions and induce endotoxemia in an in vitro model. The excessive lipid metabolite LPC and circulating LPS coordinately disrupted cholesterol metabolism and induced ER stress and apoptosis in hepatocytes (Figure 6K).

3 | DISCUSSION

To our knowledge, this is the first study using a life-course animal model to show that early-life antibiotic exposure can perturb the gut microbiota and subsequently promote metabolic dysfunction and hepatic steatosis, leading to the development of MASLD. Postnatal antibiotic exposure was a critical time period during which long duration of exposures resulted in more prominent

mean ± SEM, $n = 3$, one-way ANOVA. (D) Serum total cholesterol, triglyceride, low-density lipoprotein cholesterol (LDL-C), and cholesterol/high-density lipoprotein cholesterol (HDL-C) ratios. Data represented as mean ± SEM, $n = 5$, one-way ANOVA. (E) Representative H&E and ORO staining of the mice liver after HFD treatment. (F) Hepatic lipid deposition represented by the percentage of ORO positive-stained area as quantified by ImageJ. Data represented as mean ± SEM, based on 3 images for each group, one-way ANOVA. (G) The relative abundance of hepatic genes regulating cholesterol synthesis (HMGCR, HMGCS1, LSS), cholesterol export (ABCG1), and cholesterol utilization (CYP7A1, CYP7B1, CYP27A1) in CC and AA group after HFD treatment. Data represented as mean ± SEM, $n = 5$, Student' s *t*-test was used to determine significant differences for each gene. BF samples were collected when pups were 3 weeks old; HFD samples were collected when pups were 23 weeks old.

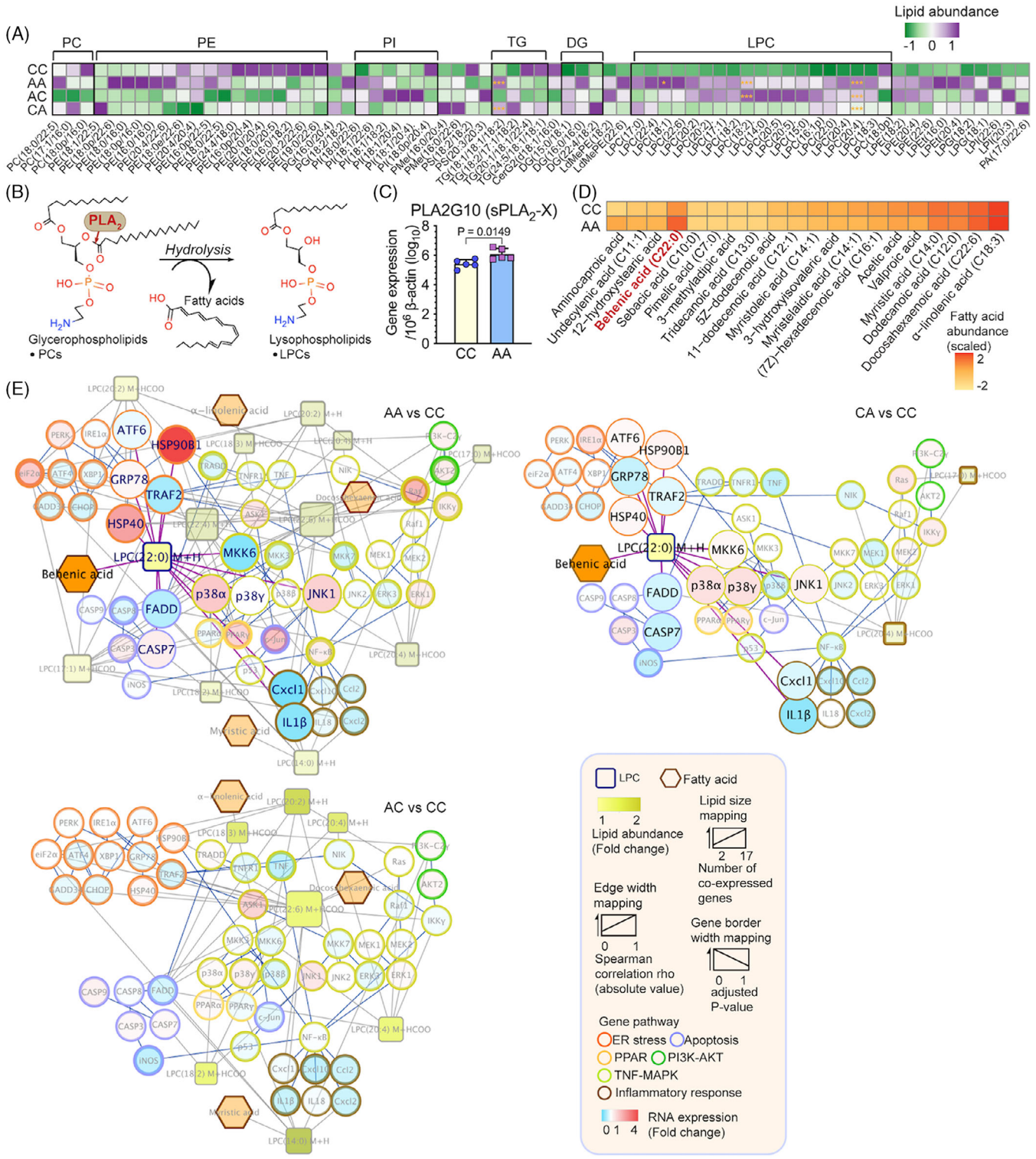

FIGURE 5 The multiomic interactive networks revealed *Parabacteroides*-modulated glycerophospholipid metabolism and the cytotoxic effect of lysophosphatidyl choline (LPC). (A) Differentially expressed lipids [abundance ratio < 0.66 or > 1.2, and variable importance in projection (VIP) > 1]. Statistical significance was determined with two-way ANOVA, $n = 5$, **p*-value < 0.05, ***p*-value < 0.01. (B) A simplified presentation of the action of PLA_2 cascade. PLA_2 enzymes catalyze the hydrolysis of the sn-2 ester bond in glycerophospholipids to produce free fatty acids and lysophospholipids. (C) Colonic expression of PLA2G10, a gene encoding group X secretory PLA_2 ($sPLA_2$-X), in mice after HFD treatment (23 weeks old). (D) Heatmap showing the relative abundance of all the fatty acids identified through serum metabolomics. The graph was made based on the mean value ($n = 3$) of the measured abundance for each metabolite. (E) Networks profiling of the *Parabacteroides*-associated lipid-gene regulation. Differentially expressed (DE) LPCs (squares) that were also closely correlated with

disruptions in intergenerational gut microbiota transfer and development of hepatic steatosis. The observed endotoxemia and metabolic dysfunctions following early-life antibiotic exposure can be mechanistically explained by the overblooming of gut *Parabacteroides* and the subsequent accumulation of LPCs with associated pathological pathways such as ER stress and apoptosis in hepatocytes. Moreover, our study showed that early-life antibiotic exposure could overcome the inherent metabolic capacity of BALB/c mice and aggravate metabolic dysfunction and hepatic steatosis.

Previous studies have shown that microbiota dysbiosis induced by low-dose penicillin in early life, rather than the antibiotic itself, can cause long-lasting metabolic consequences and excessive adiposity.[28,45] Indeed, we found that the perturbations in the gut microbiota of offspring caused by maternal antibiotic administration could be long-lasting. In dams, antibiotic administration only transiently decreased the α-diversity of the gut microbiota, which recovered upon antibiotic withdrawal. By contrast, in pups, the decrease in gut microbiota α-diversity from early-life antibiotic exposure lasted longer. In humans, the resilience of the gut microbiome against antibiotic perturbation is influenced by the state of the microbiome, diet, exposure duration, route of administration, and spectrum of antibiotic activities.[46] While the gut microbiota of healthy adults tends to be resilient to short-term broad-spectrum antibiotic interventions, those of infants respond more dramatically to antibiotic perturbations.[46–48] Subject to factors such as antibiotic dose and breastfeeding mode, the microbiome of infants can fail to completely recover for over two years after an antibiotic intervention in the first year of life.[32,46] Long-term dysregulation of childhood microbiome predisposes to multiple diseases including asthma and overweight/obesity, alongside persistent metabolic consequences.[49,50] Although the effect of penicillin on the gut microbiota has been arbitrarily considered weaker than macrolides,[49,51] our results highlight that it can still have long-term impacts on offspring following maternal administration during early life. The preexisting metabolic disorders after antibiotic exposure may potentiate into a long-term advanced disease status with synergistic impacts of adverse environmental factors.

Compared to prenatal antibiotic exposure, postnatal antibiotic exposure disrupted intergenerational gut microbiota transfer fidelity and altered early-life microbiota onset to a greater degree (Figures 2 and 3). In pups exposed to antibiotics postnatally, certain beneficial microbiota such as *Lactobacillus*[52] and *Rikenellaceae*[28] were not transferred from dams to pups and they were continuously deficient until adulthood despite several diet shifts (Figures 2A and 3B). The theory of "disappearing microbiota" has proposed an association between the gut microbes lost during vertical transmission with the epidemics of chronic diseases such as obesity.[53] The substantial impact of indirect antibiotic exposure on the offspring's gut microbiome composition could be attributable to the postnatal period being a critical period for gut microbiota development: the microbiota is seeded from mothers at birth. In human studies, intrapartum postnatal administration of antibiotics tended to more profoundly impact on infant gut colonization, leading to a decreased diversity, a decreased proportion of the phyla *Actinobacteria* and *Bacteriodetes* and increased *Proteobacteria*. By contrast, these taxonomic compositional changes and the species richness were compromised or not significant in infants born by mothers with prenatal antibiotics exposure, although potential biases on feeding mode, route of delivery, gestational age and the type and duration of antibiotic use could not be minimized in these studies.[9] Early-life antibiotic exposure could affect breast milk microbiome composition and, by extension, the offspring's gut microbiota.[54] Breastfeeding helps develop a healthy gut microbiome and reduces the risk of childhood overweight.[55] There should therefore be greater consideration into the prescription of penicillin for lactating women, as this may have eliminated the benefits of maternal breast milk and predisposed infants to metabolic dysfunction in our mice model.

We profiled the etiology of gut microbiota-associated metabolic disorders and mechanistically linked the enrichment of *Parabacteroides* in pups with postnatal antibiotic exposure in MASLD pathogenesis (Figures 3–6). Studies on *Parabacteroides* highlighted its dichotomous role in the development of metabolic disorders, depending on the administration context and strain-to-strain differences.[56–58] In our mice model, the bloom of opportunistic bacteria such as *Enterorhabdus* and

Parabacteroides were mapped to genes (circles) to draw an individual functional network showing the perturbations caused by different antibiotic exposures. All the interactions with LPC (22:0) were highlighted by an enlarged nodes and thick purple edges, while those interactions failing to show simultaneous co-expression patterns with the respective fatty acids were hidden. The sizes of all the nodes are proportional to the number of interactions within each individual network. The color of the circle's outline was mapped to the biological pathways of the genes according to KEGG pathway. Gray edges indicate the associations between LPCs and genes. The edge thickness was drawn based on the value of the correlation coefficient. Blue edges indicated the regulatory paths between genes, which were derived from the literature. All the lipid, metabolite and gene abundance were obtained from pup mice after HFD treatment (23 weeks old).

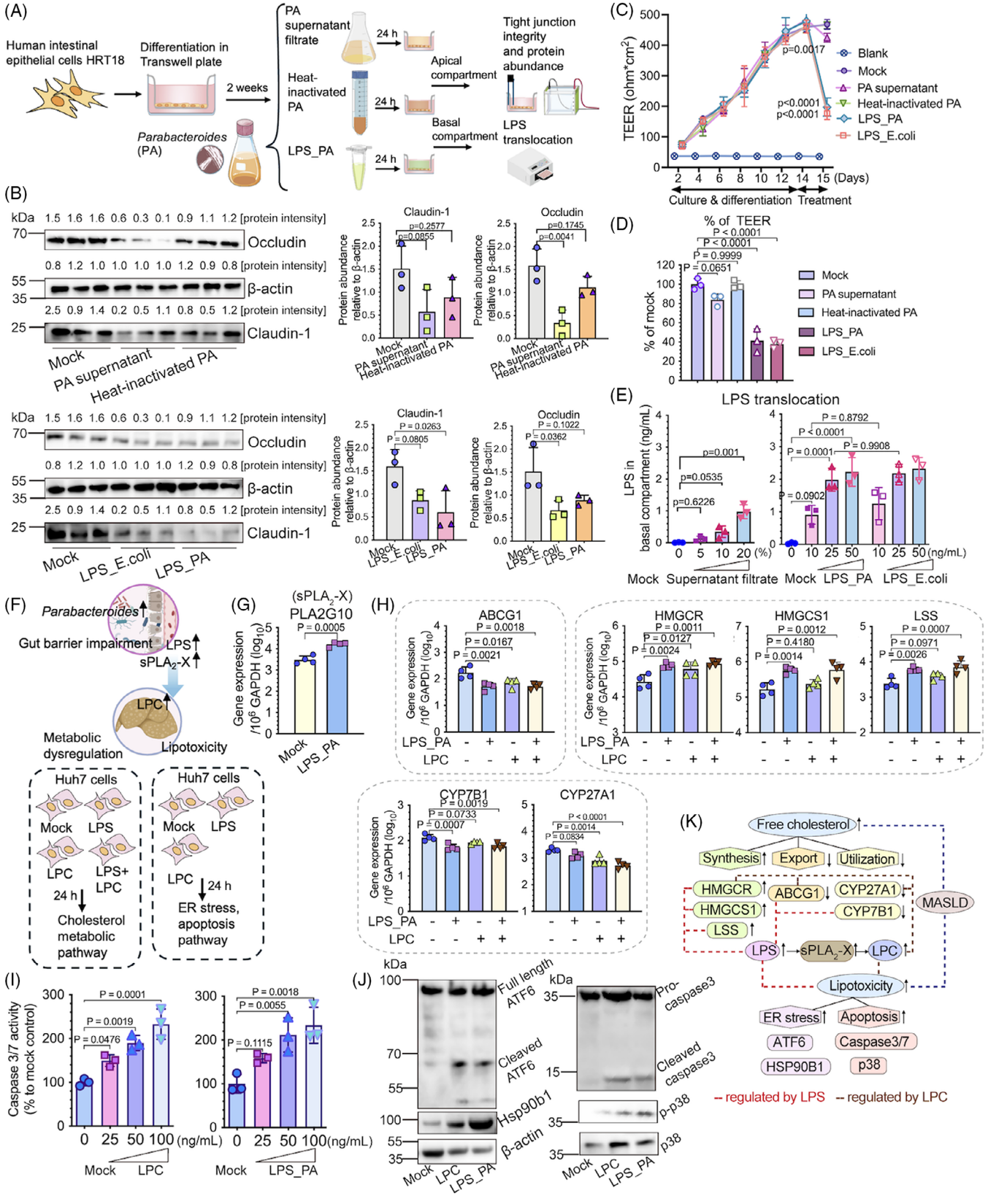

FIGURE 6 *Parabacteroides*-induced gut barrier damage and LPS release led to hepatocellular apoptosis and the perturbation of cholesterol metabolic pathways in vitro. (A) Schematic overview of the experiments examining the functional components of *Parabacteroides* that affect gut barrier function and LPS release. (B) Western blot images and protein density quantification of tight junction proteins of HRT18 cells exposed to conditioned medium (Mock), PA supernatant filtrate, heat-inactivated PA (upper panels), and LPS extracted from *E. coli* and

Parabacteroides following prolonged usage of antibiotics in early life, possibly out-competed the developmentally-beneficial microbial taxa, causing gut dysbiosis and systemic endotoxemia (Figures 3D and 4A). It has been shown that low dose LPS (as little as 1 ng/10 g of body weight) could significantly increase the lipid generation and secretion as well as the serum triglyceride in mouse models.[59] In experimental and clinical studies, the increase of *E. coli* derived LPS has been linked to in MASLD and liver damage by inducing macrophage and platelet activation through the TLR4 pathway.[60,61] This LPS-associated metabolic dysfunctions has also been observed in our study: LPS derived from the bloom of *Parabacteroides*, directly modulated cholesterol metabolism and hepatic apoptosis pathways, meanwhile elevates $sPLA_2$-X and caused the accumulation of cytotoxic LPCs (Figure 6). Specifically, our multiomic analysis pinpointed LPC (22:0) as a death effector and key driver of MASLD development (Figures 5 and 6). Given the complexity of the onset of metabolic illness following early-life antibiotic exposure, the microbial drivers including *Parabacteroides* should be comparatively studied. A detailed regulation of microbial taxa and systemic LPS pool could be profiled based on bacteria genomic and transcriptomic analysis of genes controlling the biosynthesis of LPS, to map the microbiome perturbations and LPS-associated metabolic dysfunctions.

Our study also revealed the complexity and crosstalk of metabolic dysregulations and hepatocyte damage in MASLD pathogenesis. Excessive lipids generate lipotoxicity effect and a global disturbance of hepatocellular homeostasis. Subsequently aberrant unfolded proteins accumulate within the ER membranes, causing the "ER stress." Persistent ER stress leads to unfold protein responses (UPR) and could ultimately progress into apoptosis through three stress sensors, namely, inositol-requiring enzyme 1 alpha (IRE1α), protein kinase RNA-like ER kinase (PERK), and activating transcription factor 6 (ATF6).[62] Hepatocyte apoptosis is the predominant cell death pathway in nonalcoholic steatohepatitis.[63] As ER plays an important role in regulating triglyceride and cholesterol biosynthesis,[64] UPR and apoptosis also implicate abnormal lipid synthesis.[65] In our study, postnatal and prenatal antibiotic exposure differentially activated the ER stress and apoptosis pathways to various extents. This could be explained by the various LPCs generated and their individual functions.[66] In consensus with previous reports,[41,42,67–70] we confirmed the role of LPS_PA and LPC (22:0) in triggering cell death, and augmenting MASLD pathogenesis[23] via disturbing the production, utilization and transport of cholesterol (Figure 6H-J). Direct injection of a L-α-LPC to ICR mice has been shown to induce lobular hepatitis and apoptosis at 3 days post treatment.[41] In that study, the types of available free fatty acids and inflammatory cytokines were assumed to regulate the conversion of DG into either LPC or triglyceride.[41] Here in our early-life antibiotic exposure mice model, a predominant DG→PC→LPC pathway over DG→TG pathway, alongside the defects in systemic immune development, may have shifted hepatic cell fate from survival (inflammation) toward death. Further work will be required to address the differential functions of the LPCs and the cognate fatty acids following early-life antibiotics exposure, especially in clinical settings.

Our antibiotic exposure model could be further improved in generalizability, by further investigating the timing, duration, and class of antibiotics that could differentially affect metabolic outcomes.[9,71] *Enterorhabdus* and

PA (lower panels). The protein intensity was quantified by ImageJ. The normalized ratio was labeled above the respective band and was used for the quantification of occludin and claudin-1 relative to β-actin. Data represented as mean ± SEM, $n = 3$, one-way ANOVA. (C, D) PA components-induced integrity change measured by TEER. The final resistance values are expressed as: TEER = $(R - R_b) \times A$, where R is the measured resistance of the cells, R_b is the resistance of the media blank control (no cells), and A is the area of the filter (1.12 cm^2). (E) LPS translocation measured by the amount of LPS in the basal compartment. Cells treated with 20% of conditioned medium or DMSO served as mock controls. (F) Graphical presentation of the metabolic dysfunctions and hepatocellular lipotoxicity modulated by *Parabacteroides* through the gut-liver axis. Huh7 cells were treated with DMSO, LPS_PA (50 ng/mL), LPC (22:0) (50 ng/mL), or a combination of LPS and LPC (50 ng/mL vs. 50 ng/mL) for 24 h and harvested to measure the changes of gene markers of cholesterol metabolic pathways and cell death pathways. (G) The expression of PLA2G10, a gene encoding $sPLA_2$-X in HRT18 cells with or without LPS_PA treatment. Data represented as mean ± SEM, $n = 4$, Student's t-test. (H) Expression of gene markers in cholesterol synthesis (HMGCR, HMGCS1, LSS), export (ABCG1) and utilization (CYP7B1, CYP27A1) pathways in Huh7 cells treated with DMSO, LPS_PA (50 ng/mL), LPC (22:0) (50 ng/mL), or a combination of LPS and LPC (50 ng/mL vs. 50 ng/mL). Data represented as mean ± SEM, $n = 4$, one-way ANOVA. (I) Caspase cleavage induced by LPS_PA and LPC (22:0). Data represented as mean ± SEM, $n = 4$, one-way ANOVA. (J) Western blot images showing the activation of ER stress (ATF6 cleavage and Hsp90b1 upregulation), and apoptosis (phosphorylation of p38 and caspase 3 cleavage) in Huh7 cells treated with DMSO, LPS_PA (50 ng/mL) or LPC (22:0) (50 ng/mL). (K) Schematic diagram showing the two pathogenic processes of MASLD. Endotoxemia and the accumulation of cytotoxic lipids including LPC dysregulate the synthesis, export and utilization of cholesterol, and trigger ER stress and apoptosis following the primary lipid accumulation in liver. PA, *Parabacteroides distasonis*; TEER, transepithelial electrical resistance. Icons from (A) and (F) were made using BioIcons.

Parabacteroides have been reported to coordinate with LPCs and damage the epithelial barrier in a colitis mice model.[72,73] Our study also showed similar co-expression patterns between these two taxa with LPC molecules under a synergistic effect of antibiotics and HFD (Figure S3B). While we elucidated *Parabacteroides*-mediated hepatocellular responses, further comparative and functional investigations on *Enterorhabdus* are needed. A total of 13 *Parabacteroides* species, among 20 culturable species, have been identified as inhabitants of the human intestine[74] and different species are associated to different diseases.[75,76] Therefore, species- or strain-level identification of *Parabacteroides* and their mechanistic contributions to the development of liver steatosis are warranted.

The mouse strain was used given their unique metabolic capacity driven by genetic factors, marked by the irresponsiveness of hepatic CYP7A1 to HFD treatment[36–38]; this allows us to evaluate whether early-life gut dysbiosis could modulate the intrinsically silenced metabolic processes. Here, we observed that antibiotic-induced gut dysbiosis in early life suppressed hepatic CYP7A1 in BALB/c mice, suggesting that microbiome can overcome the inherent metabolic capacity driven by the genetic determinants. However, further investigations using transgenic mice and other CYP7A1-irresponsive strains (i.e., NZB and 129/J) are needed to confirm this generalizability.[36–38] Moreover, although the functional role of the CYP7A1 gene in humans has been reported,[77,78] particularly its deficiency in hyperlipidemia,[78] the generalizability of our findings to humans needs further investigation.

Our study has several strengths. While numerous observational studies have investigated the long-term health outcomes of neonates following prenatal and postnatal antibiotic exposures, complex factors that interact with microbiome in early life continue to hinder our understanding of microbiome-driven metabolic outcomes in humans.[6,9,71] In addition, the heterogeneity among studies, different outcome measurements, and microbiota detection methods hamper the generalizability of observations.[9] Our study is the first of its kind to trace gut microbiota composition throughout the entire infancy period using an animal model and showed that microbiota-driven mechanisms aggravates metabolic dysfunction in early life, by eliminating the major confounding factors such as delivery mode and maternal diet. While effective stewardship for early-life antibiotic treatments is still an obstacle, we anticipate that our study will help inform clinical practices and health policies regarding the collateral damage of maternal antibiotic administration in early life, especially on the risk of developing MASLD. Efforts should be made toward a better use of other detection tools for bacteremia in the clinical practice, in order to avoid any prolonged antibiotic administration. Since there are currently no effective treatments for MASLD, our findings highlight potential prognostic biomarkers and the importance of early interventions using gut microbiota-targeted strategies. The integrated microbiome and multiomic framework will allow identifying more central hubs and checkpoints that could be used as preventive or therapeutic targets for MASLD.

4 | METHODS

4.1 | Mouse strain, husbandry, and treatment

Pairs of 8-week-old conventional BALB/c mice were obtained and maintained under specific pathogen-free (SPF) facilities of The Centre for Comparative Medicine Research (CCMR) to breed the study group litters. Standardized housing conditions were maintained with a 12-h light/dark cycle and ad libitum access to diet and water throughout the experiment. Dams were randomly assigned into four groups according to whether they were kept conventionally (C) or with antibiotic administrations (A): (1) with antibiotic only prenatally (AC), (2) with antibiotic only postnatally (CA), (3) with antibiotic both prenatally and postnatally (AA), and (4) conventionally from prenatal to postnatal periods (CC). Penicillin V was administered to the assigned dams via the drinking water at 0.25 mg/mL in their late pregnancy (the last week prior to laboring), late lactation period (the last week prior to weaning), or during both pregnancy and the breastfeeding period. The antibiotic supplementation was calculated by adjusting the therapeutic doses of penicillin based on comparable peak serum concentrations between a therapeutic human dose (250 mg) and an oral dose (40 mg/kg) used on animal models.[79–81] Water was refreshed every 3 days for the duration of the experiment. Dams without penicillin V treatment served as a control group. Pups were weaned at Day 21 and separated by sex to retain only males. All retained pups were then assigned into the four dam groups per their antibiotic exposure (AA: pups born by dams with both prenatal and postnatal antibiotic exposure; AC: pups born by dams with only prenatal antibiotic exposure; CA: pups born by dams with only postnatal antibiotic exposure; CC: pups born by dams without maternal antibiotic exposure). All groups of pups underwent a 10% kcal fat standard chow diet (CD) period for five weeks to obtain identical weights, before shifting to a 45% kcal fat HFD until the end of the experiment. Their body weight was monitored throughout the experiment. Ethical approval for animal experiments were obtained from the Committee on the

Use of Live Animals in Teaching and Research (CULATR 4852-18).

4.2 | Cell culture

The human intestinal epithelial cells HRT18 were maintained in RPMI-1640 (Gibco) medium supplemented with 10% fetal bovine serum (FBS) and 100 U/mL penicillin/streptomycin. Human hepatoma cell line Huh7 was cultured in Dulbecco's modified Eagle's medium (DMEM, Gibco) containing 2 % of human serum (Merck) and 100 U/mL penicillin/streptomycin since human serum cultured Huh7 cells has been reported to demonstrate more physiological relevant features in terms of fatty acid metabolism.[82]

4.3 | Fecal DNA extraction, 16S rRNA sequencing, and microbiome analysis

Fecal samples were collected from adult and infant mice, weighed, and stored with DNA/RNA Shield-fecal preservation buffer (Zymo Research) at −80°C prior to DNA extraction. Genomic DNA was extracted from fecal samples using QIAamp PowerFecal DNA Kit (Qiagen) according to manufacturer's instructions. Resulting DNA templates were subjected to 300 bp paired-end double-index Illumina sequencing approaches to target V3-V4 hypervariable regions of the 16S rRNA gene. Raw 16S rRNA sequences were analyzed using the QIIME2 pipeline.[83] Within-community diversity (α-diversity) was calculated by Chao1 and Observe ASVs. Between-sample differences of microbiota diversity (β-diversity) were assessed by Bray–Curtis dissimilarity index, tested by Permutational Multivariate Analysis of Variance (PERMANOVA) and visualized by PCoA and CCA. The LEfSE was used to identify bacterial taxa altered by early-life antibiotic exposures. We considered taxa with LDA score > 2 and $p < 0.05$ to be statistically significantly differential between groups. Associations between microbiome composition and lipids were tested using Spearman's correlation coefficient.

4.4 | Serum lipopolysaccharides, lipid biochemistry, and cytokine quantification

Sera were obtained from whole blood samples to examine LPS (Mouse LPS ELISA Kit, Cusabio), total cholesterol triglycerides (Cholesterol LiquiColor® Test, Stanbio), HDL-C (Direct HDL-Cholesterol LiquiColor® Test, Stanbio), and LDL-C following the manufacturers' respective protocols. Mice serum cytokine levels, including TNF-α, IL-2, IL-6, IL-9, IL-13, IL-17A, IL-17F, and IL-22 levels, were measured using LEGENDplex™ Mouse Th Cytokine Panel (Biolegend) according to the manufacturer's instructions. Data was acquired on an Attune™ NxT Acoustic Focusing Cytometer and analyzed with the LEGENDplex™ Data Analysis software (Biolegend) using a five-parameter logistic curve to derive the standard curve. Cytokine levels were calculated based on their respective standard curve and presented as values over the detection limit.

4.5 | Histopathological examination

Mice liver was fixed in 10% neutral-buffered formalin for hematoxylin and eosin (H&E) staining. Hepatic lipid content was determined using frozen sections stained with Oil Red O. Images were acquired on a Leica DM3000 microscope.

4.6 | Western blot

Expressions of claudin-1 and occludin were quantified by western blot analysis. Mouse anti-claudin-1 antibody (Santa Cruz Biotechnology, sc-166338), rabbit anti-occludin antibody (Abcam, ab167161), mouse anti-ATF6 antibody (Abcam, ab122897), rabbit anti-caspase-3 antibody (Abcam, ab32351), rabbit anti-Hsp90b1 (GRP94) (Abcam, ab238126), phospho-p38 MAPK antibody (Thermo Scientific, 36–8500), p38 MAPK antibody (Thermo Scientific, p38-3F11), and mouse anti-β-actin antibody (Abcam, ab8226) were used as primary antibodies for the detection of each respective target protein. Goat anti-rabbit IgG (H + L) horseradish peroxidase (HRP) conjugated antibody (Thermo Scientific, 656120) and goat anti-mouse IgG (H + L) HRP antibody (Thermo Scientific, 626520) were used as secondary antibodies in the western blot. For tissue sample processing, 2-cm sections of mid-jejunal intestine were harvested from each mouse and homogenized in 250 µL of ice-cold RIPA-buffer (Thermo Scientific, 89900) with protease inhibitor (Thermo Scientific, A32963) and ceramic beads (2.8 mm, Qiagen) by PowerLyzer 24 Homogenizer (Qiagen). This mixture was centrifuged at 12,000 $\times g$ for 10 min at 4 °C. The supernatant was collected for western blot analysis.

4.7 | Transcriptomics, lipidomics, and metabolomics

For transcriptomics, mouse livers were homogenized in Trizol and total RNA was isolated for the construction of sequencing libraries. mRNA was enriched with Oligo (dT) magnetic beads and subsequently fragmented for cDNA synthesis. The stranded and polyA-selected mRNA

libraries were sequenced on the DNBseq™ system (Beijing Genomics Institute, China) using the single-end 100 bp protocol. The clean data was mapped to the mouse reference genome (GRCm38) from the Ensembl database with STAR using default parameters.

For nontargeted lipidomics, 25 mg of mice liver was weighted, mixed with 800 μL of dichloromethane: methanol (3:1, v/v) and homogenized for lipid extraction. The homogenate was centrifuged, and the supernatant was taken for lyophilization and reconstitution. A LC-MS system consisting of Waters 2D UPLC (waters) and Q Exactive high-resolution mass spectrometer (Thermo Fisher Scientific). The raw files generated by liquid chromatography-MS/MS detection were imported into LipidSearch v.4.1 (Thermo Fisher Scientific) for lipid identification and peak alignment.

Targeted quantitative metabolomics of serum samples was performed using the HM700 metabolome detection kit (Beijing Genomics Institute, China) according to previously recorded methods.[84] Metabolites extracted from the mouse serum were analyzed using Waters UPLC I-Class Plus equipped with QTRAP 6500 Plus (SCIEX) through the Multi Reaction Monitoring, multiple reaction detection scanning (MRM) mode. Metabolite concentration was calculated by the Skyline software (MacCoss Lab Software) using default parameters for each MRM Transition's automatic identification and integration, assisting with manual inspection. The content of each substance (μmol/g) = $C \times A/m$; C = the concentration value obtained by bringing the integrated peak area of the target index in the sample into the standard curve (μmol/L); A = the dilution factor; m = the mass of the weighed solid sample (mg).

4.8 | Integrated multiomics analysis

Differentially expressed (DE) transcripts between groups were analyzed using the EdgeR statistical package. Gene clustering was performed according to our in-house pipeline to obtain the Gene Ontology (GO) terms and Kyoto Encyclopedia of Genes and Genomes (KEGG) pathways. Genes were screened by annotating their predominant functions to pathways that are closely related to MASLD pathogenesis, including the ER stress, apoptosis, inflammatory response, PI3K-AKT, TNF-MAPK, and peroxisome proliferator-activated receptor (PPAR) signaling pathways. Statistical analysis for lipidomics was performed on metaX.[85] To screen for DE lipid molecules, we evaluated the variable importance in projection (VIP) values of the first two principal components of the PLS-DA[86] and fold changes of lipid abundance. Differentially expressed lipids were defined as those with an abundance ratio of < 0.66 or > 1.2 and VIP > 1. Spearman's correlation analysis was conducted to identify the co-expression patterns between dysregulated bacterial taxa, DE lipids, and genes that had been functionally screened.

To investigate microbiota-mediated responses to HFD, fold changes of the genes and LPCs were calculated by comparing their expressions in groups exposed to antibiotics with those in the control group under HFD. Strong positive correlations (Spearman's correlation coefficient > 0.3) between microbiota and lipidomic markers and strong correlations (Spearman's correlation coefficient > 0.4 or < -0.4) between lipidomic and transcriptomic markers were selected and merged to construct an integrated network. Gene-gene interactions were identified in the literature, mapped with the fold changes, and integrated to show microbiota-mediated signaling events. Based on the principle of the hydrolysis process of glycerophospholipid mediated by PLA_2, LPCs were matched to their cognate fatty acids to further pinpoint those simultaneously elevated in mice with antibiotic exposure.

4.9 | Bacterial culture and LPS extraction

BLAST search of 31 ASV sequences of *Parabacteroides* (lengths ranging from 463 to 469 nucleotides) yielded highest identity (99.14%) to *Parabacteroides distasonis*. To prepare for representative functional components of *Parabacteroides*, in-house isolated *Parabacteroides distasonis* (PA) were anaerobically cultured in Cooked Meat Medium at 37°C overnight, to obtain cell-free supernatant filtrate, heat-inactivated bacteria, and LPS extract. The overnight culture (2×10^8 CFU/mL, 10 mL) was centrifuged at 6000 rpm for 15 min, to collect either filter-sterilized culture supernatant filtrate or sedimented bacteria. Bacterial supernatant filtrate (of around 5 ng/μL of LPS) was neutralized to pH 7.0 before use. To prepare for the heat-inactivated bacteria, the bacterial pellet was washed with PBS, sonicated for 90 s, and boiled for 10 min. The total volume was brought to 10 mL with PBS. The LPS was isolated from the bacteria pellet using LPS Extraction Kit (Boca Scientific) according to the manufacturer's instructions. The concentration of LPS was determined using LAL Chromogenic Endotoxin Quantitation Kit (Thermo Fisher). The LPS extract of *E. coli* was prepared in the similar way.

4.10 | Transepithelial electrical resistance (TEER) and LPS translocation assay

HRT18 cells were seeded onto Transwell inserts (0.4 μm pore size, 1.12 cm^2, Costar) at a density of approximately

2×10^5 cells per cm^2 and cultured for 14 days to form the tight junctions. The growth medium was supplied to both the apical and basal compartments and was replenished every other day. A Millicell ERS-2 Volt-Ohm Meter (EMD Millipore) was used to measure the TEER every other day to monitor the formation of the tight junctions. On the day of treatment, a final concentration of 20 % bacterial supernatant filtrate (of around 5 ng/μL of LPS), 20 % heat-inactivated bacterial homogenate and 50 ng/mL of LPS extract was added into the apical compartment respectively. Mock treatment group was set by supplying with an equal volume of bacteria culture medium. TEER was measured at 24 h post treatment to compare the impact of each bacterial product on the epithelial barrier integrity.

To assess the amount of LPS translocated into the basal compartment of the Transwell system, serially diluted bacterial supernatant filtrate and extracted LPS was added into the apical compartment. Cells treated with 20% of conditioned medium or DMSO served as mock controls. At 24 h post treatment, medium in the basal compartment was harvested for LPS quantification.

4.11 | Quantitative reverse transcription polymerase chain reaction (RT-qPCR)

Cells were lysed in RL buffer and extracted with the MiniBEST Universal RNA Extraction Kit (TaKaRa). RT and qPCR were performed with Transcriptor First-Strand cDNA Synthesis Kit and LightCycler 480 master mix (Roche). Primers used in RT-qPCR reactions were listed in Table S3. Human gene expression was normalized to human glyceraldehyde-3-phosphate dehydrogenase (GAPDH) mRNA, whereas the mouse gene expression was normalized to mouse β-actin mRNA. Relative gene expression was quantified using the CT ($2^{-\Delta\Delta CT}$) method.

4.12 | Caspase assay

Huh7 cells were seeded in a Corning® 96 well plate (Cat. CLS9102) and treated with LPC (22:0) (Avanti Polar Lipids) or LPS_PA under serial dilutions for 24 h. The Caspase-Glo-3/7 assay (Promega) was used to quantify the activation of executor caspases including caspase-3 and caspase-7. Cells were lysed with the Caspase-Glo-3/7 reagent at the designated time points, followed by measuring the luminescence signal with the Vector X3 multilabel plate reader (PerkinElmer).

4.13 | Statistical analyses

Statistical comparisons between different groups were made by one-way ANOVA, two-way ANOVA, or Student's *t*-test using GraphPad Prism (GraphPad Software). A p value < 0.05 was considered significant.

AUTHOR CONTRIBUTIONS

H.M.T., X.Z., and D.C.L.C. conceptualized the study and designed the experiments, with the supervision of A.K., F.K.L.C., and S.C.N. X.Z. and D.C.L.C. performed the experiments with the crucial help of D.Z.Y.S., Y.T., and W.Z. X.Z., D.C.L.C., and J.Z. analyzed the data with the assistance of H.M.T. and Y.P. X.Z. and H.M.T. wrote the manuscript. H.M.T., M.K.L.W., A.M.H., J.Y. T., A.K., F.K.L.C., and S.C.N. critically reviewed the manuscript and provided intellectual input. All authors participated in discussing and revising the manuscript. All authors have read and approved the final manuscript.

ACKNOWLEDGMENTS

We are grateful to the staff at the animal research center for their helps and we acknowledge Hilda and Kan for their contributions in animal handling. Icons from Graphical Abstract were created with biorender.com. Icons from Figure 6 were made using BioIcons. This project was partially supported by a start-up research grant and direct grant of The Chinese University of Hong Kong (CUHK) and a grand under Early Career Scheme from the Research Grants Council of the Hong Kong Special Administrative Region, China (RGC/ECS Project No. 27117022 and RGC/GRF Project No. 14113923) to H.M.T. This study and authors affiliated with MagIC are also partially supported by InnoHK, The Government of Hong Kong, Special Administrative Region of the People's Republic of China. H.M.T. is a Visiting Associate Professor of the Yong Loo Lin School of Medicine, National University of Singapore, an Honorary Associate Professor of HKU-Pasteur Research Pole, and an Adjunct Professor of the Nanjing Medical University. This study was supported by The start-up research grant and direct grant of The Chinese University of Hong Kong; Early Career Scheme and General Research Fund from the Research Grants Council of the Hong Kong Special Administrative Region, China (RGC/ECS Project No. 27117022 and 14113923); InnoHK, The Government of Hong Kong, Special Administrative Region of the People's Republic of China.

CONFLICT OF INTEREST STATEMENT

F.K.L.C. is Board Member of CUHK Medical Centre. He is a cofounder, nonexecutive Board Chairman and

shareholder of GenieBiome Ltd. He receives patent royalties through his affiliated institutions. He has received fees as an advisor and honoraria as a speaker for Eisai Co. Ltd., AstraZeneca, Pfizer Inc., Takeda Pharmaceutical Co., and Takeda (China) Holdings Co. Ltd. S.C.N. has served as an advisory board member for Pfizer, Ferring, Janssen, and Abbvie and received honoraria as a speaker for Ferring, Tillotts, Menarini, Janssen, Abbvie, and Takeda. S.C.N. has received research grants through her affiliated institutions from Olympus, Ferring, and Abbvie. S.C.N. is a scientific co-founder and shareholder of GenieBiome Ltd. S.C.N. receives patent royalties through her affiliated institutions. F.K.L.C., S.C.N., H.M.T. are named inventors of patent applications held by The CUHK and MagIC that cover the therapeutic and diagnostic use of microbiome but have no potential relevant financial or nonfinancial interests to disclose. The other authors have no conflicts of interest to declare.

DATA AVAILABILITY STATEMENT

Quality-controlled 16S rRNA sequencing data and RNA sequencing data have been deposited into the European Nucleotide Archive under BioProjects PRJEB62481 and PRJEB63629. Lipidomics data is available at https://doi.org/10.6084/m9.figshare.23309462.v1. Any additional information required to reanalyze the data reported in this paper is available upon request.

ETHICS STATEMENT

This study involving mice was approved by the Committee on the Use of Live Animals in Teaching and Research (CULATR 4852-18).

ORCID

Jie Zhu https://orcid.org/0000-0002-5789-6296

REFERENCES

1. Mueller NT, Bakacs E, Combellick J, Grigoryan Z, Dominguez-Bello MG. The infant microbiome development: mom matters. *Trends Mol Med*. 2015;21(2):109-117.
2. Rautava S, Luoto R, Salminen S, Isolauri E. Microbial contact during pregnancy, intestinal colonization and human disease. *Nat Rev Gastroenterol Hepatol*. 2012;9(12):565-576.
3. Koenig JE, Spor A, Scalfone N, et al. Succession of microbial consortia in the developing infant gut microbiome. *Proc Natl Acad Sci U S A*. 2011;108(Suppl 1):4578-4585.
4. Mueller NT, Whyatt R, Hoepner L, et al. Prenatal exposure to antibiotics, cesarean section and risk of childhood obesity. *Int J Obes (Lond)*. 2015;39(4):665-670. 10.1038/ijo.2014.180
5. Palmer C, Bik EM, DiGiulio DB, Relman DA, Brown PO. Development of the human infant intestinal microbiota. *PLoS Biol*. 2007;5(7):e177.
6. Ainonen S, Tejesvi MV, Mahmud MdR, et al. Antibiotics at birth and later antibiotic courses: effects on gut microbiota. *Pediatr Res*. 2022;91(1):154-162.
7. Le Doare K, O'driscoll M, Turner K, et al. Intrapartum antibiotic chemoprophylaxis policies for the prevention of group b streptococcal disease worldwide: systematic review. *Clin Infect Dis* 2017;65(Suppl 1):S143-S151.
8. Chung H, Pamp SJ, Hill JA, et al. Gut immune maturation depends on colonization with a host-specific microbiota. *Cell*. 2012;149(7):1578-1593. 10.1016/j.cell.2012.04.037
9. Dierikx TH, Visser DH, Benninga MA, et al. The influence of prenatal and intrapartum antibiotics on intestinal microbiota colonisation in infants: a systematic review. *J Infect*. 2020;81(3):190-204. 10.1016/j.jinf.2020.05.002
10. Maynard CL, Elson CO, Hatton RD, Weaver CT. Reciprocal interactions of the intestinal microbiota and immune system. *Nature*. 2012;489(7415):231-241.
11. Faye AS, Allin KH, Iversen AT, et al. Antibiotic use as a risk factor for inflammatory bowel disease across the ages: a population-based cohort study. *Gut*. 2023;72(4):663-670. gutjnl-2022-327845. 10.1136/gutjnl-2022-327845
12. Rinella ME, Lazarus JV, Ratziu V, et al. A multi-society Delphi consensus statement on new fatty liver disease nomenclature. *J Hepatol*. 2023;78(6):1966-1986. 10.1016/j.jhep.2023.06.003
13. Lim GEH, Tang A, Ng CH, et al. An observational data meta-analysis on the differences in prevalence and risk factors between MAFLD vs NAFLD. *Clin Gastroenterol Hepatol*. 2023;21(3):619-629.e617.
14. Friedman SL, Neuschwander-Tetri BA, Rinella M, Sanyal AJ. Mechanisms of NAFLD development and therapeutic strategies. *Nat Med*. 2018;24(7):908-922.
15. Nassir F. NAFLD: mechanisms, treatments, and biomarkers. *Biomolecules*. 2022;12(6):824. 10.3390/biom12060824
16. Huang T, Yu B, Zhou X, et al. Exploration of the link between COVID-19 and alcoholic hepatitis from the perspective of bioinformatics and systems biology. *MedComm*. 2023;2(1):e42.
17. Lim GEH, Nakanishi N, Kawai T, et al. An observational data meta-analysis on the differences in prevalence and risk factors between MAFLD vs NAFLD. *Clin Gastroenterol Hepatol*. 2021;21(3):619-629.e617.
18. Martin-Mateos R, Albillos A. The role of the gut-liver axis in metabolic dysfunction-associated fatty liver disease. *Front Immunol*. 2021;12:660179.
19. Zeybel M, Arif M, Li X, et al. Multiomics analysis reveals the impact of microbiota on host metabolism in hepatic steatosis. *Adv Sci (Weinh)*. 2022;e2104373.
20. Hamilton MK, Boudry G, Lemay DG, Raybould HE. Changes in intestinal barrier function and gut microbiota in high-fat diet-fed rats are dynamic and region dependent. *Am J Physiol Gastrointest Liver Physiol*. 2015;308(10):G840-851.
21. Brun P, Castagliuolo I, Leo VDi, et al. Increased intestinal permeability in obese mice: new evidence in the pathogenesis of nonalcoholic steatohepatitis. *Am J Physiol Gastrointest Liver Physiol*. 2007;292(3):G518-525.
22. Cani PD, Amar J, Iglesias MA, et al. Metabolic endotoxemia initiates obesity and insulin resistance. *Diabetes*. 2007;56(8):1761-1772.
23. Min HK, Kapoor A, Fuchs M, et al. Increased hepatic synthesis and dysregulation of cholesterol metabolism is associated with the severity of nonalcoholic fatty liver disease. *Cell Metab*. 2012;15(5):665-674.

24. Van Rooyen DM, Larter CZ, Haigh WG, et al. Hepatic free cholesterol accumulates in obese, diabetic mice and causes nonalcoholic steatohepatitis. *Gastroenterology*. 2011;141(4):1393-1403.e1391-1395.
25. Henkel A, Green RM. The unfolded protein response in fatty liver disease. *Semin Liver Dis*. 2013;33(4):321-329.
26. Musso G, Cassader M, Paschetta E, Gambino R. Bioactive lipid species and metabolic pathways in progression and resolution of nonalcoholic steatohepatitis. *Gastroenterology*. 2018;155(1):282-302.e288.
27. Cho I, Yamanishi S, Cox L, et al. Antibiotics in early life alter the murine colonic microbiome and adiposity. *Nature*. 2012;488(7412):621-626.
28. Cox LM, Yamanishi S, Sohn J, et al. Altering the intestinal microbiota during a critical developmental window has lasting metabolic consequences. *Cell*. 2014;158(3):705-721.
29. Wang L, Wang S, Zhang Q, et al. The role of the gut microbiota in health and cardiovascular diseases. *Mol Biomed*. 2022;3(1):30.
30. Trasande L, Blustein J, Liu M, et al. Infant antibiotic exposures and early-life body mass. *Int J Obes (Lond)*. 2013;37(1):16-23.
31. Ajslev TA, Andersen CS, Gamborg M, Sorensen TI, Jess T. Childhood overweight after establishment of the gut microbiota: the role of delivery mode, pre-pregnancy weight and early administration of antibiotics. *Int J Obes (Lond)*. 2011;35(4):522-529.
32. Korpela K, Salonen A, Virta LJ, et al. Association of early-life antibiotic use and protective effects of breastfeeding: role of the intestinal microbiota. *JAMA Pediatr*. 2016;170(8):750-757.
33. Imoto N, Kano C, Aoyagi Y, et al. Administration of beta-lactam antibiotics and delivery method correlate with intestinal abundances of Bifidobacteria and Bacteroides in early infancy, in Japan. *Sci Rep*. 2021;11(1):6231.
34. Clavenna A, Bonati M. Differences in antibiotic prescribing in paediatric outpatients. *Arch Dis Child*. 2011;96(6):590-595.
35. Schulfer AF, Battaglia T, Alvarez Y, et al. Intergenerational transfer of antibiotic-perturbed microbiota enhances colitis in susceptible mice. *Nat Microbiol*. 2018;3:234-242.
36. Carter CP, Howles PN, Hui DY. Genetic variation in cholesterol absorption efficiency among inbred strains of mice. *J Nutr*. 1997;127:1344-1348.
37. Dueland S, France D, Wang SL, Trawick JD, Davis RA. Cholesterol 7alpha-hydroxylase influences the expression of hepatic apoA-I in two inbred mouse strains displaying different susceptibilities to atherosclerosis and in hepatoma cells. *J Lipid Res*. 1997;38:1445-1453.
38. Kirk EA, Moe GL, Caldwell MT, et al. Hyper- and hyporesponsiveness to dietary fat and cholesterol among inbred mice: searching for level and variability genes. *J Lipid Res*. 1995;36:1522-1532.
39. Kumashiro N, Erion DM, Zhang D, et al. Cellular mechanism of insulin resistance in nonalcoholic fatty liver disease. *Proc Natl Acad Sci U S A*. 2011;108:16381-16385.
40. Dial EJ, Tran DM, Romero JJ, Zayat M, Lichtenberger LM. A direct role for secretory phospholipase A2 and lysophosphatidylcholine in the mediation of LPS-induced gastric injury. *Shock*. 2010;33:634-638.
41. Han MS, Park SY, Shinzawa K, et al. Lysophosphatidylcholine as a death effector in the lipoapoptosis of hepatocytes. *J Lipid Res*. 2008;49:84-97.
42. Takahashi M, Okazaki H, Ogata Y, et al. Lysophosphatidylcholine induces apoptosis in human endothelial cells through a p38-mitogen-activated protein kinase-dependent mechanism. *Atherosclerosis*. 2002;161:387-394.
43. Cha MH, Lee SM, Jung J. Lysophosphatidylcholine induces expression of genes involved in cholesterol biosynthesis in THP-1 derived macrophages. *Steroids*. 2018;139:28-34.
44. Buzzetti E, Pinzani M, Tsochatzis EA. The multiple-hit pathogenesis of non-alcoholic fatty liver disease (NAFLD). *Metabolism*. 2016;65:1038-1048.
45. Cox LM, Blaser MJ. Pathways in microbe-induced obesity. *Cell Metab*. 2013;17:883-894.
46. Schwartz DJ, Langdon AE, Dantas G. Understanding the impact of antibiotic perturbation on the human microbiome. *Genome Med*. 2020;12:82.
47. Palleja A, Mikkelsen KH, Forslund SK, et al. Recovery of gut microbiota of healthy adults following antibiotic exposure. *Nat Microbiol*. 2018;3:1255-1265.
48. Stewart CJ, Ajami NJ, O'brien JL, et al. Temporal development of the gut microbiome in early childhood from the TEDDY study. *Nature*. 2018;562:583-588.
49. Korpela K, Salonen A, Virta LJ, et al. Intestinal microbiome is related to lifetime antibiotic use in Finnish pre-school children. *Nat Commun*. 2016;7:10410.
50. Vangay P, Ward T, Gerber JS, Knights D. Antibiotics, pediatric dysbiosis, and disease. *Cell Host Microbe*. 2015;17:553-564.
51. Bar-Oz B, Bulkowstein M, Benyamini L, et al. Use of antibiotic and analgesic drugs during lactation. *Drug Saf*. 2003;26:925-935.
52. Million M, Angelakis E, Paul M, et al. Comparative meta-analysis of the effect of *Lactobacillus* species on weight gain in humans and animals. *Microb Pathog*. 2012;53:100-108.
53. Blaser MJ. The theory of disappearing microbiota and the epidemics of chronic diseases. *Nat Rev Immunol*. 2017;17:461-463.
54. Yan W, Luo B, Zhang X, Ni Y, Tian F. Association and occurrence of bifidobacterial phylotypes between breast milk and fecal microbiomes in mother-infant dyads during the first 2 years of life. *Front Microbiol*. 2021;12:669442.
55. Woo JG, Martin LJ. Does breastfeeding protect against childhood obesity? Moving beyond observational evidence. *Curr Obes Rep*. 2015;4:207-216.
56. Wei W, Wong CC, Jia Z, et al. *Parabacteroides* distasonis uses dietary inulin to suppress NASH via its metabolite pentadecanoic acid. *Nat Microbiol*. 2023;8:1534-1548.
57. Zhao Q, Dai M-Y, Huang R-Y, et al. *Parabacteroides* distasonis ameliorates hepatic fibrosis potentially via modulating intestinal bile acid metabolism and hepatocyte pyroptosis in male mice. *Nat Commun*. 2023;14:1829.
58. Ezeji JC, Sarikonda DK, Hopperton A, et al. *Parabacteroides* distasonis: intriguing aerotolerant gut anaerobe with emerging antimicrobial resistance and pathogenic and probiotic roles in human health. *Gut Microbes*. 2021;13:1922241.
59. Feingold KR, Staprans I, Memon Ra, et al. Endotoxin rapidly induces changes in lipid metabolism that produce hypertriglyceridemia: low doses stimulate hepatic triglyceride production while high doses inhibit clearance. *J Lipid Res*. 1992;33:1765-1776.
60. d'Hennezel E, Abubucker S, Murphy LO, Cullen TW. Total lipopolysaccharide from the human gut microbiome silences Toll-like receptor signaling. *mSystems*. 2017;2.

61. Carpino G, Del Ben M, Pastori D, et al. Increased liver localization of lipopolysaccharides in human and experimental NAFLD. *Hepatology*. 2020;72:470-485.
62. Han J, Kaufman RJ. The role of ER stress in lipid metabolism and lipotoxicity. *J Lipid Res*. 2016;57:1329-1338. doi:10.1194/jlr.R067595
63. Hirsova P, Gores GJ. Death receptor-mediated cell death and proinflammatory signaling in nonalcoholic steatohepatitis. *Cell Mol Gastroenterol Hepatol*. 2014;1:17-27.
64. Huang H, Guo S, Chen Ya-Q, et al. Increased RTN3 phenocopies nonalcoholic fatty liver disease by inhibiting the AMPK-IDH2 pathway. *MedComm*. 2023;4:e226.
65. Tam AB, Roberts LS, Chandra V, et al. The UPR activator ATF6 responds to proteotoxic and lipotoxic stress by distinct mechanisms. *Dev Cell*. 2018;46:327-343.e327.
66. Jones BE, Lo CR, Liu H, et al. Hepatocytes sensitized to tumor necrosis factor-alpha cytotoxicity undergo apoptosis through caspase-dependent and caspase-independent pathways. *J Biol Chem*. 2000;275:705-712.
67. Diczfalusy U, Olofsson KE, Carlsson A-M, et al. Marked upregulation of cholesterol 25-hydroxylase expression by lipopolysaccharide. *J Lipid Res*. 2009;50:2258-2264.
68. Feingold KR, Hardardottir I, Memon R, et al. Effect of endotoxin on cholesterol biosynthesis and distribution in serum lipoproteins in Syrian hamsters. *J Lipid Res*. 1993;34:2147-2158.
69. Memon RA, Moser AH, Shigenaga JK, Grunfeld C, Feingold KR. In vivo and in vitro regulation of sterol 27-hydroxylase in the liver during the acute phase response. Potential role of hepatocyte nuclear factor-1. *J Biol Chem*. 2001;276:30118-30126.
70. Shridas P, Bailey WM, Gizard F, et al. Group X secretory phospholipase A2 negatively regulates ABCA1 and ABCG1 expression and cholesterol efflux in macrophages. *Arterioscler Thromb Vasc Biol*. 2010;30:2014-2021.
71. Pacifici GM. Placental transfer of antibiotics administered to the mother: a review. *Int J Clin Pharmacol Ther*. 2006;44:57-63.
72. Tang X, Wang W, Hong G, et al. Gut microbiota-mediated lysophosphatidylcholine generation promotes colitis in intestinal epithelium-specific Fut2 deficiency. *J Biomed Sci*. 2021;28:20.
73. Xu HM, Huang H-Li, Liu Y-Di, et al. Selection strategy of dextran sulfate sodium-induced acute or chronic colitis mouse models based on gut microbial profile. *BMC Microbiol*. 2021;21:279.
74. Cui Y, Zhang L, Wang X, et al. Roles of intestinal *Parabacteroides* in human health and diseases. *FEMS Microbiol Lett*. 2022;369.
75. Liu S, Qin P, Wang J. High-fat diet alters the intestinal microbiota in streptozotocin-induced type 2 diabetic mice. *Microorganisms*. 2019;7.
76. Kverka M, Zakostelska Z, Klimesova K, et al. Oral administration of *Parabacteroides* distasonis antigens attenuates experimental murine colitis through modulation of immunity and microbiota composition. *Clin Exp Immunol*. 2011;163:250-259.
77. Ferrell JM, Boehme S, Li F, Chiang JY. Cholesterol 7alpha-hydroxylase-deficient mice are protected from high-fat/high-cholesterol diet-induced metabolic disorders. *J Lipid Res*. 2016;57:1144-1154.
78. Pullinger CR, Eng C, Salen G, et al. Human cholesterol 7alpha-hydroxylase (CYP7A1) deficiency has a hypercholesterolemic phenotype. *J Clin Invest*. 2002;110:109-117.
79. Leclercq S, Mian FM, Stanisz AM, et al. Low-dose penicillin in early life induces long-term changes in murine gut microbiota, brain cytokines and behavior. *Nat Commun*. 2017;8:15062.
80. Nobel YR, Cox LM, Kirigin FF, et al. Metabolic and metagenomic outcomes from early-life pulsed antibiotic treatment. *Nat Commun*. 2015;6:7486.
81. Kukolja S, Wright WE, Quay JF, et al. Oral absorption of cephalosporin antibiotics. 1. Synthesis, biological properties, and oral bioavailability of 7-(arylacetamido)-3-chloro cephalosporins in animals. *J Med Chem*. 1988;31:1987-1993.
82. Gunn PJ, Green CJ, Pramfalk C, Hodson L. In vitro cellular models of human hepatic fatty acid metabolism: differences between Huh7 and HepG2 cell lines in human and fetal bovine culturing serum. *Physiol Rep*. 2017;5.
83. Bolyen E, Rideout JR, Dillon MR, et al. Reproducible, interactive, scalable and extensible microbiome data science using QIIME 2. *Nat Biotechnol*. 2019;37:852-857.
84. Liu R, Hong J, Xu X, et al. Gut microbiome and serum metabolome alterations in obesity and after weight-loss intervention. *Nat Med*. 2017;23:859-868.
85. Wen B, Mei Z, Zeng C, Liu S. metaX: a flexible and comprehensive software for processing metabolomics data. *BMC Bioinformatics*. 2017;18:183.
86. Westerhuis JA, Hoefsloot HCJ, Smit S, et al. Assessment of PLSDA cross validation. *Metabolomics*. 2008;4:81-89.

SUPPORTING INFORMATION

Additional supporting information can be found online in the Supporting Information section at the end of this article.

How to cite this article: Zhang X, Chan DCL, Zhu J, et al. Early-life antibiotic exposure aggravates hepatic steatosis through enhanced endotoxemia and lipotoxic effects driven by gut *Parabacteroides*. *MedComm*. 2025;6:e70104. https://doi.org/10.1002/mco2.70104